



HAL
open science

Simulation of Co-60 uptake on stainless steel and alloy 690 using the OSCAR V1.4 code integrating an advanced dissolution-precipitation model

Frederic Dacquait, Jerome Francescato, Etienne Tevissen, J-Baptiste Genin,
Dominique You, Chloé Cherpin, Francois Broutin

► To cite this version:

Frederic Dacquait, Jerome Francescato, Etienne Tevissen, J-Baptiste Genin, Dominique You, et al.. Simulation of Co-60 uptake on stainless steel and alloy 690 using the OSCAR V1.4 code integrating an advanced dissolution-precipitation model. Nuclear Engineering and Design, 2023, 405, pp.112190. 10.1016/j.nucengdes.2023.112190 . cea-04216336

HAL Id: cea-04216336

<https://cea.hal.science/cea-04216336v1>

Submitted on 24 Sep 2023

HAL is a multi-disciplinary open access archive for the deposit and dissemination of scientific research documents, whether they are published or not. The documents may come from teaching and research institutions in France or abroad, or from public or private research centers.

L'archive ouverte pluridisciplinaire **HAL**, est destinée au dépôt et à la diffusion de documents scientifiques de niveau recherche, publiés ou non, émanant des établissements d'enseignement et de recherche français ou étrangers, des laboratoires publics ou privés.

Simulation of Co-60 uptake on stainless steel and alloy 690 using the OSCAR v1.4 code integrating an advanced dissolution-precipitation model

Frédéric Dacquait^{1*}, Jérôme Francescato¹, Etienne Tevissen¹, Jean-Baptiste Genin¹,
Dominique You², Chloé Cherpain¹, François Broutin¹

¹ CEA, DES, IRESNE, DTN, Cadarache, F-13108 Saint-Paul Lez Durance, France.

² CEA, DES, ISAS, DPC, Saclay, F-91191 Gif-sur-Yvette, France.

* Corresponding author. E-mail address: frederic.dacquait@cea.fr

Highlights

- A dissolution-precipitation model for activated corrosion products (ACPs) in nuclear cooling systems is defined.
- This model is implemented in a simulation tool called OSCAR designed to simulate ACPs.
- An experiment performed by Studsvik Nuclear AB was simulated using the OSCAR code.
- The OSCAR code accurately reproduces the impacts of the pH, Zn injection and flow regime on the uptake of soluble ⁶⁰Co on stainless steel and alloy 690.

Abstract

The contamination of a nuclear cooling system by activated corrosion products (ACPs) is a process that involves many different mechanisms all interacting with each other. One of the most important mechanisms is dissolution-precipitation. This governs the transfer of soluble corrosion products between the circulating water and the immobile oxidized surfaces, and is strongly dependent on the water chemistry. The dissolution-precipitation model was improved in version 1.4 of the OSCAR computer code, which simulates the ACPs transfer in nuclear reactor systems. The OSCAR v1.4 code is now able to better calculate the incorporation of minor species (e.g., a cobalt isotope) into oxides using the chemistry module, PHREEQCEA, which determines the composition of an ideal solid solution and the equilibrium concentrations of elements in the aqueous solution. This model was challenged by comparing the results obtained using OSCAR v1.4 with the experimental results of a test performed in a dedicated loop by Studsvik Nuclear AB. Finally, with this model, the OSCAR v1.4 code accurately reproduces soluble ⁶⁰Co uptake on stainless steel and alloy 690 under various experimental conditions (pH, Zn injection and flow rate).

Keywords

Dissolution-precipitation; Modelling; Activated corrosion product; Nuclear reactor; Simulation

Nomenclature

$A_{n/-n}$	pre-exponential factor for dissolution-precipitation reaction of solid phase n [$\text{mol.m}^{-2}.\text{s}^{-1}$]
C_{part}	particle concentration [kg.m^{-3}]
C^θ	standard molality ($C^\theta = 1 \text{ mol.kg}_w^{-1}$)
C^{elt}	concentration of soluble element in the coolant bulk [kg.m^{-3}]
C_{wall}^{elt}	concentration of soluble element in the fluid at the wall [kg.m^{-3}]
C_{eq}^{elt}	equilibrium concentration of soluble element in the fluid at the wall [kg.m^{-3}]
C^N	molality of a chemical element [mol.kg_w^{-1}]
C_{eq}^N	equilibrium molality of a chemical element [mol.kg_w^{-1}]
D_{dep}^{elt}	diffusion coefficient of soluble element in the open porosity of the deposit / outer oxide layer [$\text{m}^2.\text{s}^{-1}$]
D_H	hydraulic diameter [m]
E_{eros}	erosion coefficient [s^{-1}]
Ea_n	activation energy of dissolution-precipitation reaction of solid phase n [J.mol^{-1}]
elt	metallic element
f_{medium}^i	mass fraction of isotope i in the considered medium [kg.kg^{-1}]

f_{rel}^i	mass fraction of isotope i involved in the release [kg.kg ⁻¹]
$f_{medium}^{i,elt}$	isotopic mass fraction of isotope i of element elt in the considered medium [kg.kg ⁻¹]
$f_{medium}^{N,i,elt}$	isotopic molar fraction of isotope i of element elt in the considered medium [mol.mol ⁻¹]
h	mass transfer coefficient of particles or ions in the fluid between the bulk and the deposit / outer oxide wall [m.s ⁻¹]
h'	mass transfer coefficient of ions in the fluid between the bulk and the particle wall [m.s ⁻¹]
i	isotope of an element
$J_{transfer}^{i/elt}$	mass transfer rate of isotope i or element elt between 2 media or 2 regions or 2 isotopes or elements [kg.s ⁻¹]
$k_{n/-n}$	surface dissolution-precipitation reaction rate constant of solid phase n [mol.m ⁻² .s ⁻¹]
L_{dep}	characteristic length of diffusion in the open porosity of the deposit / outer oxide layer [m]
$MA_{n(s)}$	single solid phase n containing metallic element M
M	metallic element (M = Co, Cr, Fe, Mn, Ni, Zn, Ag, Zr or Cu in OSCAR v1.4)
$M_{(aq)}$	soluble element M in the aqueous phase
M_{elt}	molar mass of element elt [kg.mol ⁻¹]
m^i	mass of isotope i [kg]
m_{eros}	mass of the deposit that can be eroded [kg]
m^{elt}	mass of element elt [kg.m ⁻²]
N^{elt}	number of moles of element elt [mol.m ⁻²]
$P_{p,n}$	chemical product related to solid phase n
P^θ	standard pressure ($P^\theta = 1 \text{ bar}^1$)
p_{H_2/O_2}	partial pressure of dihydrogen or dioxygen [bar]
$R_{r,n}$	chemical reactant related to solid phase n
R	universal gas constant (8.314 J.K ⁻¹ .mol ⁻¹)
$R_{solid-fluid}^{elt}$	transfer resistance of element elt at the interface solid-fluid [s.m ⁻¹]
$R_{wall-bulk}^{fluid}$	transfer resistance of soluble element elt in the fluid between the wall and the bulk [s.m ⁻¹]
Re	Reynolds number [-]
r_n	net reaction rate of dissolution-precipitation [mol.m ⁻² .s ⁻¹]
$S_{dissol/precip}$	dissolution or precipitation surface [m ²]
S_w	wet surface [m ²]
$S_{nucleat}^{spec}$	specific surface of nucleation [m ² .kg ⁻¹]
S_{part}^{spec}	specific surface of particles [m ² .kg ⁻¹]
t	time [s]
T	absolute temperature [K]
V_{cor}	surface corrosion rate [kg.m ⁻² .s ⁻¹]
V_{dissol_n}	dissolution surface reaction rate of solid phase n [mol.m ⁻² .s ⁻¹]
V_{precip_n}	precipitation surface reaction rate of solid phase n [mol.m ⁻² .s ⁻¹]
V_{rel}	surface release rate [kg.m ⁻² .s ⁻¹]
v_{depos}	deposition velocity of particles [m.s ⁻¹]
v_{dissol}^{elt}	dissolution velocity of element elt [m.s ⁻¹]

Greek symbols

α_n	molar fraction of solid phase n containing element elt relative to all solid phases containing element elt [mol.mol ⁻¹]
$\zeta_{MA_{n(s)}}$	molar fraction of $MA_{n(s)}$ ($\zeta_{MA_{n(s)}} = 1$)
μ	partial order of reaction [-]
ν	stoichiometric coefficient [-]
$\Theta_{phases(elt)}$	molar fraction in the oxide of all the solid phases n containing element elt [mol.mol ⁻¹]
Ψ_{eros}	erosion resistance coefficient [-]

¹ 1 bar = 10⁵ Pa

1. Introduction

Predicting the radioactive contamination of nuclear reactor systems is a significant challenge for plant designers and operators (occupational radiation exposure, plant availability and environment). To address this challenge, the French strategy has been focusing on:

1. Performing experiments in test loops such as the CEA loops SOZIE (Plancque et al., 2008) and CIRENE (Girard et al., 2012) mainly to obtain base data;
2. Measuring the contamination of pressurized water reactor (PWR) systems, in particular using the EMECC system designed by the CEA (Eimecke and Anthoni, 1988) to obtain on-site data;
3. Developing a simulation code, called OSCAR², to predict nuclear system contamination.

The OSCAR code was developed by the CEA (the French Alternative Energies and Atomic Energy Commission) in collaboration with EDF and Framatome, with several versions having been released since the 1970s. Its final version resulted from the merging of two previous codes in 2008 (Genin et al., 2010): PACTOLE for activated corrosion products (ACPs) and PROFIP for actinides and fission products (Beslu and Leuthrot, 1990). The OSCAR code is not only used to perform numerical simulations and predict nuclear system contamination, but it also combines and organizes all new knowledge needed to make further progress in this field. Other codes have been developed in the world (IAEA, 2012). We have chosen to focus on ACPs in this paper.

The contamination of a nuclear cooling system by ACPs involves many different mechanisms that all interact with each other (Rodliffe et al., 1987). One of the most important mechanisms is dissolution-precipitation. This governs the transfer of soluble corrosion products between the circulating water and the immobile oxidized surfaces; it is also strongly dependent on the water chemistry. To better calculate the incorporation of minor species (e.g., a cobalt isotope) into oxides, the dissolution-precipitation model was improved in version 1.4 of the OSCAR code released in 2017.

After a general presentation of the OSCAR v1.4 code, the new dissolution-precipitation model and its ability to reproduce an experimental campaign performed by Studsvik Nuclear AB are described. Lastly, a discussion of the results is presented.

2. OSCAR code modelling

2.1. PWR contamination principle

The process governing the formation of ACPs in a PWR primary system is complex and involves several interacting mechanisms (Rodliffe et al., 1987). The main source of ACPs is the uniform and generalized corrosion of the base metal composing components in contact with the primary coolant. This results in the formation of a double layer of oxide for stainless steels and Ni-based alloys (see, e.g., (Rodliffe et al., 1987) or (Marchetti-Sillans, 2007)): a compact inner Cr-rich layer and an outer porous Fe-Ni-rich layer. The inner layer is passive, which limits the exchange of ions between the base metal and the primary coolant, but without preventing it completely; some ions are directly released into the primary coolant (see, e.g., (Rodliffe et al., 1987) or (Marchetti-Sillans, 2007)). The primary coolant transports the ions produced by corrosion-release or by the dissolution of oxides. When the coolant becomes oversaturated in corrosion products (depending on the local temperature and chemical conditions), the soluble species precipitate on either the system surfaces or nucleation sites to form particles. Particles are also generated by the erosion or spalling of deposits on the system walls. When transported by the primary coolant, these particles can deposit on all the primary system surfaces. Two main sources produce ACPs by neutron activation: 1) corrosion product deposits on in-core components (mainly on fuel rod cladding³), 2) in-core components (mainly the direct activation of in-vessel internals). After being released by corrosion-release, dissolution, erosion or spalling, ACPs are transported by forced convection towards the ex-core regions and build up on system surfaces leading to an ionizing radiation field around PWR systems.

² Acronym for “Outil de Simulation de la Contamination en Réacteur” in French or “tOol for Simulating ContAmination in Reactors” in English.

³ Deposit on fuel rod cladding is also called fuel crud.

2.2. Modelling of nuclear systems

The OSCAR code modelling is based on the arrangement of control volumes (also called regions) defined by a hydraulic diameter and a wet surface. A reactor primary system or a testing loop is nodalized into as many regions as necessary defined according to their geometric, thermohydraulic, neutronic, material and operating characteristics (see an example of the OSCAR nodalization of a PWR in Figure 1).

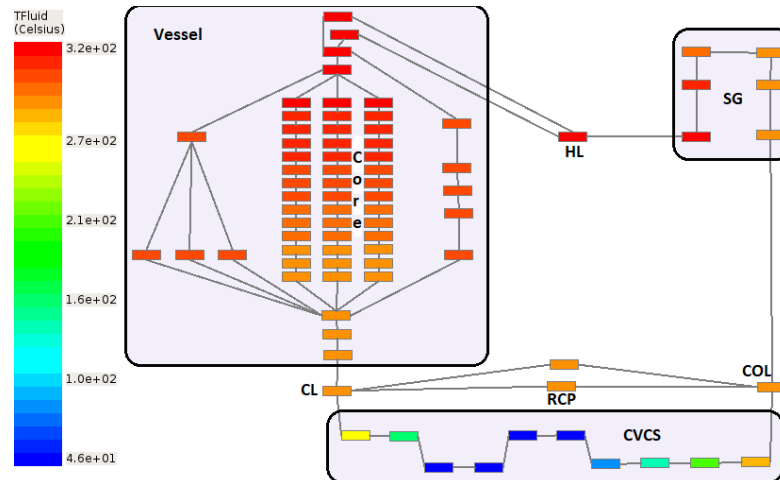


Figure 1. OSCAR v1.4 - Nodalization of a typical PWR with third-core reload fuel management (a total of 79 control volumes including 42 for the core) (HL: Hot Leg / SG: Steam Generator / COL: CrossOver Leg / RCP: Reactor Coolant Pump / CL: Cold Leg / CVCS: Chemical and Volume Control System).

Several media can be defined in each control volume (see Figure 2):

- Immobile media:
 - o Base metal: material composing the system components (stainless steel, Ni alloy, Co alloy, etc.),
 - o Inner oxide layer: a non-porous rough Cr-rich layer, which completely coats the base metal,
 - o Deposit / Outer oxide layer: a porous rough Fe-Ni-rich layer, which coats the inner oxide layer.
- Moving media due to the coolant advection:
 - o Particles: we assume that the particles are spherical and that their grain size distribution follows a log-normal law,
 - o Solubles: dissolved species.
- Trapping media for the coolant purification in the CVCS:
 - o Filter for particles,
 - o Ion-exchange resins (IER) for soluble.

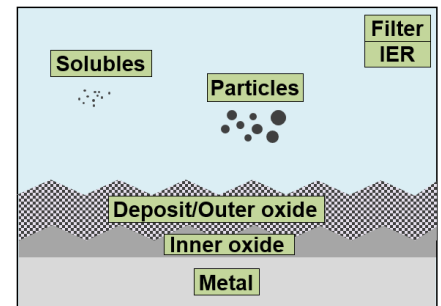


Figure 2. OSCAR v1.4 - Media taken into account in the modelling.

2.3. Chemical elements and isotopes

The main chemical elements taken into account in the OSCAR code are those composing the materials of the reactor nuclear systems that generate the main ACPs: Fe, Ni, Cr, Co, Mn. Some stable isotopes of these chemical elements become radioactive when subjected to a neutron flux. For example, the main ACPs contributing to the dose rates in the environment of a French PWR primary system are ^{58}Co and ^{60}Co (Dacquait et al., 2004). They are mainly formed by the following neutron activation reactions: $^{58}\text{Ni}(n,p)^{58}\text{Co}$ and $^{59}\text{Co}(n,\gamma)^{60}\text{Co}$.

The OSCAR code can process other elements, i.e.: Zn to describe its effect on contamination (Tigeras et al., 2008), Ag and Sb to simulate radioactive pollution by ^{110m}Ag and ^{124}Sb (Bretelle et al., 2002) (Dacquait et al.,

2016), Zr the main constituent of the PWR fuel rod cladding and Cu for fusion reactors (Dacquit et al., 2020)⁴. Adding a new soluble chemical element to the OSCAR code requires entering its thermochemical data into the OSCAR chemistry module database (see section 2.4.4) and its neutron activation rate into the OSCAR neutron database. Note that the OSCAR v1.4 code can also calculate the volume activities of coolant activation products: ¹⁶N and ⁴¹Ar.

The radioactive half-lives of the radioisotopes taken into account in the OSCAR code range from some seconds to some million years (Dacquit et al., 2021)⁵.

2.4. Mass balance and transfer mechanisms

The OSCAR code calculation kernel solves a system of mass balance equations for all isotopes (stable and radioactive) in all media in all regions at each adaptive time step (from some seconds to some days) using the following equation (Marchetto, 2002):

$$\partial m^i / \partial t = \sum_{sources} J_{transfer}^i - \sum_{sinks} J_{transfer}^i \quad \text{Eq. (1)}$$

where m^i is the mass of isotope i in a given medium [kg], t the time [s] and $J_{transfer}^i$ a transfer mass rate of isotope i between 2 media or 2 regions or 2 isotopes [kg.s⁻¹].

Thus, the OSCAR code calculates the masses of corrosion products and the activities of ACPs in the solid and liquid phases of nuclear systems as a function of time during normal operation over several decades and during transients down to a few seconds.

The transfer mechanisms taken into account in OSCAR V1.4 are indicated in the yellow boxes in Figure 3.

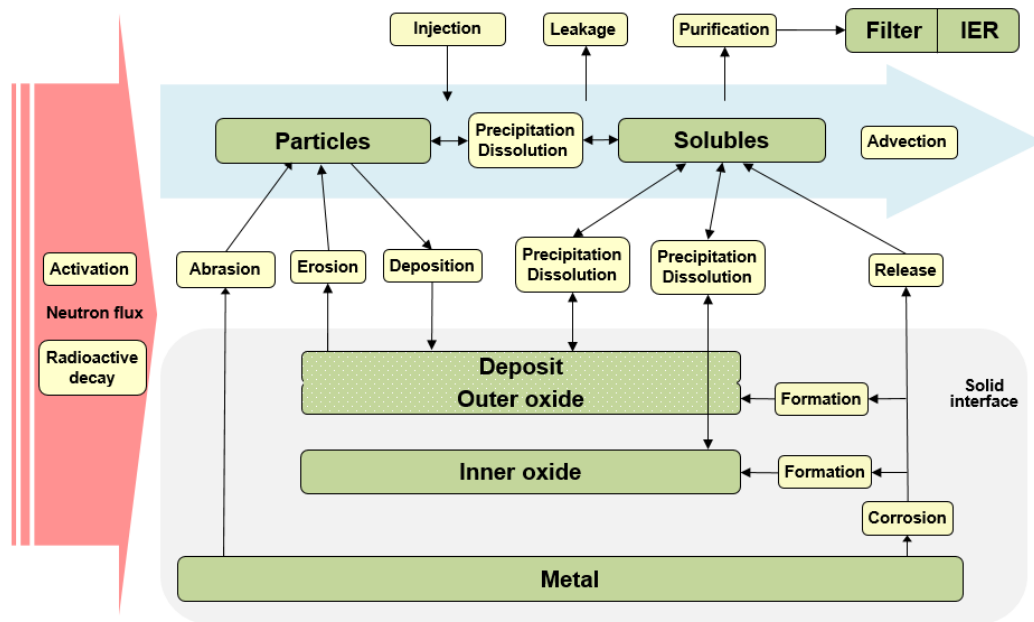


Figure 3. Mass transfer mechanisms included in the OSCAR v1.4 code.

The dissolution-precipitation model apart (see section 2.4.4), the models of the other main mechanisms, i.e. corrosion-release, erosion, and deposition, are briefly presented below.

⁴ The OSCAR code is also used for water cooling systems in fusion reactors (OSCAR-Fusion version).

⁵ The OSCAR code can be used for nuclear reactor dismantling situations.

2.4.1. Corrosion-release

Corrosion of the base metal causes the formation of an inner oxide layer (mainly chromite), of an outer oxide (ferrite and Ni^o or NiO in general) and a direct ion release into the coolant (see section 2.1). The corrosion and release rates of isotope i , $J_{corrosion}^i$ and $J_{release}^i$ [kg.s⁻¹], are given by:

$$J_{corrosion}^i = f_{met}^i S_w V_{cor} \quad \text{and} \quad J_{release}^i = f_{rel}^i S_w V_{rel} \quad \text{Eq. (2) and (3)}$$

where f_{met}^i is the mass fraction of isotope i in the metal, f_{rel}^i the mass fraction of isotope i involved in the release, S_w the wet surface [m²], V_{cor} and V_{rel} the surface corrosion and release rates respectively [kg.m⁻².s⁻¹] calculated by an empirical model as a function of the chemistry, temperature, material, manufacturing process and time (called Moorea law) or calculated by a time power law, time logarithmic law or constant value per stage.

2.4.2. Erosion

Erosion of a deposit results from the coolant friction forces. The erosion mass rate of isotope i , $J_{erosion}^i$ [kg.s⁻¹], is given by:

$$J_{erosion}^i = f_{dep}^i m_{eros} E_{eros} / \Psi_{eros} \quad \text{Eq. (4)}$$

where f_{dep}^i is the mass fraction of isotope i in the deposit / outer oxide layer, m_{eros} the mass of the deposit that can be eroded [kg], E_{eros} is the erosion coefficient [s⁻¹] based on the Cleaver and Yates model (Cleaver and Yates, 1972) depending on the shear stress at the wall and the dynamic viscosity of the coolant, and Ψ_{eros} the erosion resistance coefficient.

2.4.3. Deposition

The deposition mass rate of particles takes into account:

- Laminar (Poulson, 1983) and turbulent (Beal, 1970) diffusion (mass transfer coefficient h [m.s⁻¹]),
- sedimentation for horizontal components (Michell, 1970),
- thermophoresis for temperature gradients between the coolant and the walls (Ponting and Rodliffe, 1983),
- Nucleate boiling deposition (Ferrer, 2013).

The deposition mass rate of isotope i , $J_{deposition}^i$ [kg.s⁻¹], is given by:

$$J_{deposition}^i = f_{part}^i S_w v_{depos} C_{part} \quad \text{Eq. (5)}$$

where f_{part}^i is the mass fraction of isotope i in the particles, v_{depos} the deposition velocity of particles [m.s⁻¹], and C_{part} the particle concentration [kg.m⁻³].

It should be noted that any system defects, such as elbows or cross-section changes, disturb the hydraulic conditions and affect exchanges between the walls and the fluid stream. This effect can be taken into account in the code by the distance from the disturbance corresponding to the relaxation length, L_{relax} :

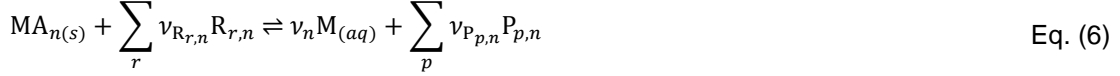
- in laminar flow via the mass transfer coefficient (Lévêque correlation): $1.614(ReScD_h/L_{relax})^{0.33} D_B/D_h$ where Re is the Reynolds number, Sc the Schmidt number, D_h the hydraulic diameter and D_B the Brownian diffusion coefficient;
- in turbulent flow via the Reynolds number used in the pressure drop coefficient: $Re^{0.75} L_{relax}/D_h$.

2.4.4. Dissolution-precipitation

The dissolution-precipitation model was reviewed for version 1.4 of the OSCAR code released in 2017.

2.4.4.1 Assumptions and justification

Consider the following elementary dissolution-precipitation surface reaction of single solid phase n containing metallic element M (M = Co, Cr, Fe, Mn, Ni, Zn, Ag, Sb, Zr or Cu in OSCAR v1.4):



where $MA_{n(s)}$ is single solid phase n containing metallic element M (e.g., main single solid phases containing Ni in OSCAR v1.4: $NiCr_2O_4$, $NiFe_2O_4$, NiO , $Ni(s)$), $M_{(aq)}$ is element M in the aqueous phase, R are the chemical reactants (H^+ , H_2 or O_2), P are the chemical products and ν are the stoichiometric coefficients.

For instance, in PWR reducing conditions, the elementary dissolution-precipitation reactions of cobalt ferrite and cobalt chromite phases ($M = Co$) considered by the OSCAR v1.4 code are written as follows:



For solid phase n , the net reaction rate of dissolution-precipitation, r_n [$mol.m^{-2}.s^{-1}$], is:

$$r_n = V_{dissol_n} - V_{precip_n} \quad \text{Eq. (9)}$$

where V_{dissol_n} and V_{precip_n} are the surface reaction rates of dissolution and precipitation respectively [$mol.m^{-2}.s^{-1}$] of solid phase n containing metallic element M , which can be written:

$$V_{dissol_n} = k_n \zeta_{MA_{n(s)}} \prod_r (C_{Rr,n}^N / C^\theta)^{\mu_{Rr,n}} \quad \text{Eq. (10)}$$

$$V_{precip_n} = k_{-n} (C_{M(aq)}^N / C^\theta)^{\mu_n} \prod_p (C_{Pp,n}^N / C^\theta)^{\mu_{Pp,n}} \quad \text{Eq. (11)}$$

where k_n and k_{-n} are the surface dissolution and precipitation, respectively, reaction rate constants of solid phase n [$mol.m^{-2}.s^{-1}$] only depending on temperature according to the Arrhenius equation $k_n = A_n e^{-Ea_n/(RT)}$ and $k_{-n} = A_{-n} e^{-Ea_{-n}/(RT)}$ with $A_{n/-n}$ and $Ea_{n/-n}$ the pre-exponential factor [$mol.m^{-2}.s^{-1}$] and the activation energy [$J.mol^{-1}$] for dissolution/precipitation reactions respectively of solid phase n , R the universal gas constant [$J.K^{-1}.mol^{-1}$] and T the absolute temperature [K], $\zeta_{MA_{n(s)}}$ is the molar fraction of the single solid phase ($\zeta_{MA_{n(s)}} = 1$), C^N are the molalities of $M_{(aq)}$ at the wall and of the chemical reactants and products [$mol.kg_w^{-1}$], C^θ is the standard molality ($C^\theta = 1 mol.kg_w^{-1}$) and μ are the partial orders of reaction for the different species.

By assuming that the partial order of reaction for $M_{(aq)}$ is 1 ($\mu_n = 1$) and the dissolution/precipitation reactions of each of solid phase n are independent from one another (heterogeneous mixture of the single solid phases in the solid), then the overall surface reaction rate of element M for the n solid phases containing element (elt) M , dN_S^{elt}/dt [$mol.m^{-2}.s^{-1}$], is:

$$\frac{dN_S^{elt}}{dt} = \sum_n \alpha_n \nu_n r_n = \sum_n \alpha_n \nu_n k_n \zeta_{MA_{n(s)}} \prod_r \left(\frac{C_{Rr,n}^N}{C^\theta} \right)^{\mu_{Rr,n}} - \frac{C_{M(aq)}^N}{C^\theta} \sum_n \alpha_n \nu_n k_{-n} \prod_p \left(\frac{C_{Pp,n}^N}{C^\theta} \right)^{\mu_{Pp,n}} \quad \text{Eq. (12)}$$

where α_n is the molar fraction of solid phase n containing element elt relative to all solid phases containing element elt .

And for isotope i of element M , we have:

$$\frac{dN_S^{i,elt}}{dt} = \sum_n \alpha_n \nu_n k_n f_{solid}^{N,i,elt} \zeta_{MA_{n(s)}} \prod_r \left(\frac{C_{Rr,n}^N}{C^\theta} \right)^{\mu_{Rr,n}} - f_{fluid}^{N,i,elt} \frac{C_{M(aq)}^N}{C^\theta} \sum_n \alpha_n \nu_n k_{-n} \prod_p \left(\frac{C_{Pp,n}^N}{C^\theta} \right)^{\mu_{Pp,n}} \quad \text{Eq. (13)}$$

where $f_{solid}^{N,i,elt}$ and $f_{fluid}^{N,i,elt}$ are the isotopic molar fractions of isotope i of element M in the solid and in the fluid respectively.

For element M , at equilibrium $dN_S^{elt}/dt = 0$, then we have:

$$\sum_n (\alpha_n)_{eq} \nu_n k_{-n} \prod_p (C_{Pp,n}^N / C^\theta)_{eq}^{\mu_{Pp,n}} = (C^\theta / C_{M(aq)}^N)_{eq} \sum_n (\alpha_n)_{eq} \nu_n k_n \prod_r (C_{Rr,n}^N / C^\theta)_{eq}^{\mu_{Rr,n}} \quad \text{Eq. (14)}$$

For the reactions regarding the solid phases of corrosion products in PWR conditions, we consider that (a) the And concentrations of reactants or products (H^+ , H_2 or O_2) are set by the CVCS, (b) the concentration of a metallic element other than element M in a mixed oxide is close to its equilibrium concentration in the coolant and (c) the solid composition to reach equilibrium does not practically vary. Therefore, we can write: $(C_{R,r,n}^N)_{eq} \cong C_{R,r,n}^N$, $(C_{P,p,n}^N)_{eq} \cong C_{P,p,n}^N$ and $(\alpha_n)_{eq} \cong \alpha_n$. By combining Eq. (12) and (14) we obtain:

$$dN_S^{elt}/dt = \sum_n \alpha_n \nu_n k_n \prod_r (C_{R,r,n}^N / C^\theta)^{\mu_{R,r,n}} \left(1 - C_{M(aq)}^N / C_{M(aq)_{eq}}^N\right) \quad \text{Eq. (15)}$$

for isotope i of element M, we have:

$$dN_S^{i,elt}/dt = \sum_n \alpha_n \nu_n k_n \prod_r (C_{R,r,n}^N / C^\theta)^{\mu_{R,r,n}} \left(f_{solid}^{N,i,elt} - f_{fluid}^{N,i,elt} C_{M(aq)}^N / C_{M(aq)_{eq}}^N\right) \quad \text{Eq. (16)}$$

For metallic element M, from Eq. (15) we can define the dissolution-precipitation surface mass rate, dm_S^{elt}/dt [$\text{kg}\cdot\text{m}^{-2}\cdot\text{s}^{-1}$]:

$$dm_S^{elt}/dt = M_{elt} \sum_n \alpha_n \nu_n k_n (10^{-pH})^{\mu_{H^+,n}} \left(p_{H_2/O_2} / P^\theta\right)^{\mu_{H_2/O_2,n}} \left(1 - C_{wall}^{elt} / C_{eq}^{elt}\right) \quad \text{Eq. (17)}$$

where M_{elt} is the molar mass [$\text{kg}\cdot\text{mol}^{-1}$] of element M, pH is the pH at the wall temperature, p_{H_2} or p_{O_2} and P^θ are the dihydrogen or dioxygen partial pressure [bar] and the standard pressure ($P^\theta = 1$ bar) respectively, C_{wall}^{elt} is the concentration [$\text{kg}\cdot\text{m}^{-3}$] of element $M_{(aq)}$ in the coolant at the wall and C_{eq}^{elt} is the equilibrium concentration [$\text{kg}\cdot\text{m}^{-3}$] of element $M_{(aq)}$ in the coolant at the wall.

Eq. (17) can be written in this form:

$$dm_S^{elt}/dt = v_{dissol}^{elt} (C_{eq}^{elt} - C_{wall}^{elt}) \quad \text{Eq. (18)}$$

where $v_{dissol}^{elt} = \frac{M_{elt}}{C_{eq}^{elt}} \sum_n \alpha_n \nu_n V_{dissol,n}$ is called the dissolution velocity of element M [$\text{m}\cdot\text{s}^{-1}$], with $V_{dissol,n} = k_n (10^{-pH})^{\mu_{H^+,n}} \left(p_{H_2/O_2} / P^\theta\right)^{\mu_{H_2/O_2,n}}$.

As a function of the concentration of element $M_{(aq)}$ in the coolant bulk, C^{elt} [$\text{kg}\cdot\text{m}^{-3}$], we could easily demonstrate that:

$$dm_S^{elt}/dt = \frac{1}{R_{solid-wall} + R_{wall-bulk}} (C_{eq}^{elt} - C^{elt}) \quad \text{Eq. (19)}$$

where $R_{solid-wall} = 1/v_{dissol}^{elt}$ is the dissolution resistance [$\text{s}\cdot\text{m}^{-1}$] and $R_{wall-bulk}$ is the transfer resistance in the fluid between the wall and the bulk [$\text{s}\cdot\text{m}^{-1}$] using an analogy with a network of resistances in an electrical circuit. Eq. (19) is commonly used in the modelling of the behaviour of corrosion products in the PWR primary system (see, e.g., (Rodliffe et al., 1987)).

Finally, the dissolution-precipitation surface mass rate of isotope i of element M, dm_S^i/dt in [$\text{kg}\cdot\text{m}^{-2}\cdot\text{s}^{-1}$], is:

$$dm_S^i/dt = \frac{1}{\frac{1}{v_{dissol}^{elt}} + R_{wall-bulk}} \left(f_{solid}^{i,elt} C_{eq}^{elt} - f_{fluid}^{i,elt} C^{elt}\right) \quad \text{Eq. (20)}$$

where $f_{solid}^{i,elt} = m_{solid}^{i,elt} / m_{solid}^{elt}$ and $f_{fluid}^{i,elt} = m_{fluid}^{i,elt} / m_{fluid}^{elt}$ are the isotopic mass fractions of isotope i of element M in the solid and in the fluid respectively.

Note that:

- The precipitation rate is expressed with the dissolution kinetic constants

- The relation between the dissolution velocity of an element, v_{dissol}^{elt} in $[m.s^{-1}]$, and the dissolution surface reaction rate of solid phases containing this element, V_{dissol_n} in $[mol.m^{-2}.s^{-1}]$, is $v_{dissol}^{elt} = M_{elt}/C_{eq}^{elt} \sum_n \alpha_n v_n V_{dissol_n}$
- For an element, if $(C_{eq}^{elt} - C^{elt}) > 0$ there is dissolution, if $(C_{eq}^{elt} - C^{elt}) < 0$ there is precipitation
- For an isotope, if $(f_{solid}^{ielt} C_{eq}^{elt} - f_{fluid}^{ielt} C^{elt}) > 0$ there is dissolution, if $(f_{solid}^{ielt} C_{eq}^{elt} - f_{fluid}^{ielt} C^{elt}) < 0$ there is precipitation
- $\sum_{ielt} (f_{solid}^{ielt} C_{eq}^{elt} - f_{fluid}^{ielt} C^{elt}) = C_{eq}^{elt} - C^{elt}$
- An isotope can precipitate even in unsaturated conditions of the chemical element, i.e. $(C_{eq}^{elt} - C^{elt}) > 0$, if $(f_{solid}^{ielt} C_{eq}^{elt} - f_{fluid}^{ielt} C^{elt}) < 0$. In this case, it corresponds to an isotope exchange.

2.4.4.2 OSCAR expression

From Eq. (20), the dissolution-precipitation mass rate of isotope i of element elt , $J_{dissol/precip}^i$ $[kg.s^{-1}]$, is expressed in the OSCAR modelling as follows:

$$J_{dissol/precip}^i = \frac{S_{dissol/precip}}{R_{solid-fluid}^{elt} + R_{wall-bulk}^{fluid}} \left| f_{solid}^{ielt} C_{eq}^{elt} - f_{fluid}^{ielt} C^{elt} \right| \quad \text{Eq. (21)}$$

where $S_{dissol/precip}$ is the dissolution or precipitation surface $[m^2]$, $R_{solid-fluid}^{elt}$ the transfer resistance of element elt at the interface solid-fluid $[s.m^{-1}]$, $R_{wall-bulk}^{fluid}$ the transfer resistance of soluble element elt in the fluid between the wall and the bulk $[s.m^{-1}]$, f_{solid}^{ielt} and f_{fluid}^{ielt} the isotopic mass fractions of isotope i of element elt in the considered solid medium (Inner oxide, Deposit / Outer oxide or Particle) and in the fluid respectively, C_{eq}^{elt} the equilibrium concentration of elt in the coolant at the considered solid wall $[kg.m^{-3}]$, and C^{elt} the concentration of soluble elt in the coolant bulk $[kg.m^{-3}]$.

For the deposit / outer oxide and the inner oxide, it is considered that the precipitation surface is the wet surface of the considered medium and the dissolution surface is the wet surface of the solid phases containing element elt of the considered medium. Concerning the deposit / outer oxide, $S_{precip} = S_w$ and $S_{dissol} = S_w \theta_{\Sigma n}$ where $\theta_{\Sigma n}$ is the molar fraction in the oxide of all the solid phases n containing element elt . Concerning the inner oxide, these surfaces are multiplied by the open porosity of the deposit / outer oxide layer. For the particles, It is considered that the precipitation surface depends on the specific surface of nucleation, $S_{nucleat}^{spec}$ $[m^2.kg_w^{-1}]$, and the dissolution surface depends on the specific surface of particles, S_{part}^{spec} $[m^2.kg^{-1}]$.

$R_{solid-fluid}^{elt} = 1/v_{dissol}^{elt}$ where $v_{dissol}^{elt} = \frac{M_{elt}}{C_{eq}^{elt}} \sum_n \alpha_n v_n V_{dissol_n}$ is the dissolution velocity of element elt $[m.s^{-1}]$

(considering a heterogeneous mixture of single solid phases) with $V_{dissol_n} = k_n (10^{-pH})^{\mu_{H^+n}} (p_{H_2/O_2})^{\mu_{H_2/O_2n}}$ the dissolution surface reaction rate of solid phase n containing element elt $[mol.m^{-2}.s^{-1}]$ and $k_n = A_n e^{-Ea_n/(RT)}$ the dissolution surface kinetic constant of solid phase n $[mol.m^{-2}.s^{-1}]$. M_{elt} is the molar mass of element elt $[kg.mol^{-1}]$, α_n the molar fraction of solid phase n containing element elt relative to all solid phases containing element elt , v_n the stoichiometric number of element elt in solid phase n , A_n the pre-exponential factor $[mol.m^{-2}.s^{-1}]$ and Ea_n the activation energy $[J.mol^{-1}]$ for the dissolution of solid phase n , R the universal molar gas constant $(8.314 J.mol^{-1}.K^{-1})$, T the wall or bulk coolant temperature $[K]$, pH the pH calculated at the wall or bulk coolant temperature, p_{H_2/O_2} the dihydrogen or dioxygen partial pressure $[bar]$, $\mu_{j,n}$ the partial orders of dissolution reaction of solid phase n for the different species j .

For the deposit / outer oxide, $R_{wall-bulk}^{fluid} = 1/h$ where h is the mass transfer coefficient of soluble element elt $[m.s^{-1}]$ in the fluid between the deposit / outer oxide wall and the bulk calculated using the same formula as those used for particle deposition (see section 2.4.3). For the inner oxide layer, $R_{wall-bulk}^{fluid} = L_{dep}/D_{dep}^{elt} + 1/h$ with $L_{dep} = \tau_{dep} e_{dep}$ the characteristic length of diffusion $[m]$ where τ_{dep} and e_{dep} are the tortuosity and thickness of the deposit / outer oxide, and $D_{dep}^{elt} = D_{liq}^{elt} \varepsilon_{dep} / \tau_{dep}$ the diffusion coefficient of soluble elt $[m^2.s^{-1}]$ in the open porosity of the deposit / outer oxide where D_{liq}^{elt} is the liquid diffusion coefficient of soluble elt at the wall temperature and

ε_{dep} the porosity of the deposit / outer oxide. For the particles, $R_{wall-bulk}^{fluid} = 1/h'$ where h' is the mass transfer coefficient of soluble element elt [$m.s^{-1}$] in the fluid between the particle wall and the bulk (Rodliffe et al., 1987). The OSCAR chemistry module, PHREEQCEA⁶, and a CEA thermodynamic database gathering experimental, extrapolated and literature data (Plancque et al., 2011) are used to calculate the thermodynamic equilibrium concentration of each element in the coolant C_{eq}^{elt} , the molar fraction of each solid phase α_n (solid speciation), the pH at temperature, and the dihydrogen or dioxygen partial pressure p_{H_2} or p_{O_2} . At each time step, PHREEQCEA determines the composition of the ideal solid solution (mixed oxides) and pure solid phases (Ni° or NiO_s generally in PWR conditions) and the equilibrium concentration of each element in the coolant assuming thermodynamic equilibrium in the coolant with respect to the chemical conditions (pH and redox potential), the wall or bulk coolant temperature, and the masses of metallic elements in the considered solid (inner oxide or deposit / outer oxide and particles) calculated by the OSCAR calculation kernel in each control volume.

2.5. Calibration and validation methodology

The transfer mechanisms need to be calibrated because there are unknown values of some parameters from the physical models presented above. For the dissolution-precipitation model, the surface dissolution reaction rate constants k_n , the activation energies Ea_n and the reaction orders μ for the different solid phases n (ferrites, chromites, Ni° , etc.) are hardly known in PWR conditions (up to 340 °C, 155 bar). The surface dissolution reaction rate constant of Ni° and NiO was calibrated according to the simulation of a typical PWR in power operation. For cobalt ferrites and chromites, the surface dissolution reaction rate constants, $k_{CoFe_2O_4}$ and $k_{CoCr_2O_4}$, and the proton reaction orders, $\mu_{H^+,CoFe_2O_4}$ and $\mu_{H^+,CoCr_2O_4}$, are determined by simulating an experiment carried out by Studsvik (see section 3). Simulating a typical PWR cold shutdown enables us to adjust the activation energies and the reaction orders, $\mu_{H^+,n}$, $\mu_{H_2,n}$ and $\mu_{O_2,n}$. The erosion coefficient, E_{eros} , was calibrated according to the simulation of a typical PWR in power operation (Dacquait et al., 2018) and the particle deposition model was adjusted by simulating an experiment in the CEA CIRENE loop (Girard et al., 2012).

After calibrating the physical models using test loops and a standard French PWR, global validation of the OSCAR v1.4 code was ensured by comparing the simulation of the power operation for several cycles and cold shutdowns of 6 PWR units with different operating and design characteristics (900/1300/1450 MWe PWRs, alloy 600MA/600TT/690TT SG tubing, alloy 718/Zry spacer grids, target $pH_{300^\circ C}$ of 7.0/7.2, different fuel management strategies, with or without steam generator replacement, etc.) with contamination measurements in these 6 PWRs. The calibration and the validation of OSCAR was also possible thanks to the wealth of operating experience (OPEX) collected from the EMECC⁷ assessments. To date, about 430 EMECC campaigns have been performed by the CEA in 76 different French and foreign PWRs since 1971 (Dacquait et al., 2004). In addition to the γ surface activities measured using the EMECC device (Eimecke and Anthoni, 1988), the OSCAR results have been compared to other on-site measurements: volume activities and chemical element concentrations⁸.

To use OSCAR, it is first necessary to provide a set of input data by using an input graphical user interface (GUI):

- Geometric and thermal-hydraulic data of each control volume: hydraulic diameter (D_H), wet surface, fluid velocity, flowrate, bulk and wall coolant temperatures;
- Material characteristics: initial composition, initial thickness, density, roughness and tortuosity. Any possible surface treatment is taken into account via the experimental corrosion and release rates;
- Neutronic data: nuclear power fraction in each region of the vessel. The neutron reaction rates, as a function of PWR type, fuel burn-up, ²³⁵U enrichment and Pu content, are extracted from a nuclear database interfaced with OSCAR;

⁶ A version of the PHREEQC code (Parkhurst and Appelo, 2013) extended to cover the PWR temperature range. The main modification is in the dependency of the equilibrium constant with the temperature (Plancque et al., 2011):

$$K(T) = a_1 + a_2T + \frac{a_3}{T} + a_4 \log T + \frac{a_5}{T^2} + \frac{a_6}{T^3} + \left(a_7 + \frac{a_8}{T} + \frac{a_9}{T^2} \right) \log_{10} \frac{\rho_w(T)}{1000}$$

where a_i are parameters to fit with the HKF interaction constants $\log_{10,HKF}(T,P)$ at $P = P_{sat}$ and ρ_w is the water density at T .

⁷ French acronym for “Ensemble de Mesures et d’Étude de la Contamination des Circuits”.

⁸ On-site dose rate measurements are not considered because not only do they reflect the surface and volume activities, but they also depend on the radionuclide activity levels, the measured components, the measurement conditions, and the ambient dose rates.

- Operating data: nominal power, boron, lithium, dihydrogen and dioxygen concentrations as a function of time. A Zn injection rate can also be defined;
- Reloading of components: a part of core regions for refuelling at each end of operating cycle, steam generators in case of their replacement, etc.
- Purification: efficiency of the filter and ion exchange resins for the CVCS.
- It is possible to simulate an entire cold shutdown procedure by varying the nominal power, pressure, temperature, flowrate, boron, lithium and dihydrogen and dioxygen concentrations. Otherwise, only the results of a cold shutdown are taken into account in the calculation.

The OSCAR results are plotted using an output GUI. These results include masses, activities, dose rates, transfer mass rates, chemistry parameters (equilibrium concentrations, solid speciation, pH_T, partial pressures, dissolution surface reaction rates, dissolution velocities, etc.) and thermal hydraulic parameters (density, viscosity, Reynolds number, Schmidt number, mass transfer coefficient, etc.).

3. OSCAR code simulation of a Studsvik test

3.1. Description of the experiment

Studsvik Nuclear AB performed tests in a dedicated experimental loop (Öijerholm et al., 2014) to study the impact of different parameters such as the pH, Zn, flow velocity and materials on ⁶⁰Co uptake in PWR conditions. One of these tests, campaign A, described in (Öijerholm et al., 2016), has been simulated using the OSCAR v1.4 code.

The specimen stage (see Figure 4) consists of 2 parallel-tube assemblies (A and B). In each tube assembly, three specimens are exposed to the passing flow in the following sequence: stainless steel (SS) 304L (tube 1), alloy 690 (tube 2) and SS 304L (tube 3). The flow regime is laminar in tubes 1 and 2 whereas it is turbulent in tube 3 (reduced inner diameter). The system is described as “once-through” heated to 285 °C by a pre-heater partly made from alloy 690 tubes. The water chemistry reflects the real PWR exposure conditions, and the pH_{300°C} varies between 6.9 and 7.6 during the test (see Table 1 and Figure 5). After 200 h of exposure, Zn is injected into the tube assembly A (concentration of 10 ppb). Soluble ⁶⁰Co (radiotracer) and Co are added (volume activity of 200 Bq/kg for ⁶⁰Co and concentration of 9 ppt for Co) just upstream of the specimen stage and the uptake of ⁶⁰Co on each individual tube is monitored on-line by mobile NaI gamma detectors. The test lasts 47 days.

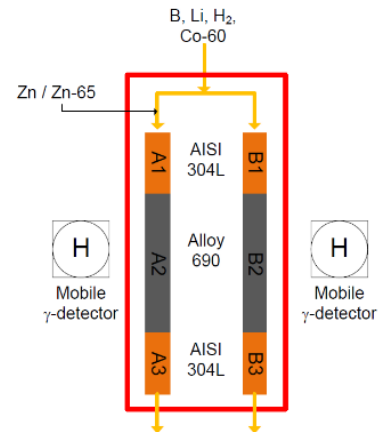


Figure 4. Studsvik test section (figure from (Öijerholm et al., 2016))

Table 1. Studsvik test - Exposure conditions (table from (Öijerholm et al., 2016)).

Parameter	Campaign A
Temperature (°C)	285
pH ₃₀₀	6.9 – 7.6
pH _{air}	6.7 – 7.4
B (ppm)	700
Li (ppm)	1.23 – 6.75
H ₂ (ml/kg H ₂ O)	45
Co-60 (Bq/kg)	200
Total dosed Co (ppb)	0.009
Zn-dosage (ppb)	10
Zn-65 (Bq/l)	49
Flow rate (kg/h)	6
Flow velocity (m/s)	0.005 / 0.74

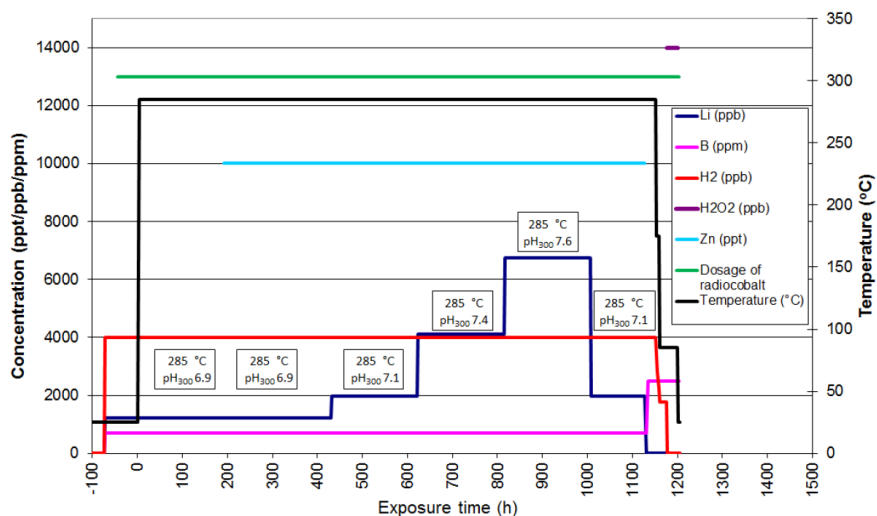


Figure 5. Studsvik test - Exposure in campaign A (figure from (Öijerholm et al., 2016)).

The tube characteristics are given in Table 2. Note that the Co content of SS304L is unknown (the data was neither provided by the manufacturer, nor measured by Studsvik Nuclear AB).

Table 2. Studsvik test - Tube characteristics (from (Öijerholm et al., 2014) and (Öijerholm et al., 2016)).

Material	Tube #	Length (mm)	Inner diameter (mm)	Flow velocity (m.s ⁻¹)	Re	Treatment before test
Alloy 690	2	500	16.87	0.005	700	Cleaning with acetone in ultrasonic bath
SS 304L	1	300	17.0	0.005	700	
	3		1.4	0.74	8000	

Abbreviated check analysis of Alloy 690 specimen material.								Abbreviated check analysis of the SS 304L specimen material								
Material	Elemental composition (weight %)							Material	Elemental composition (weight %)							
	Mn	Si	Cr	Ni	Co	Ti	Fe		C	Mn	Si	P	S	Ni	Cr	Fe
Alloy 690	0.27	0.2	29.7	Bal.	0.007	0.32	9.7	304L	0.013	1.65	0.47	0.030	0.012	10.5	18.72	Bal.

3.2. Description of the OSCAR simulation

The Studsvik testing loop is nodalized into 11 regions (see Figure 6):

- 6 regions for the two 3-tube assemblies A [A1_SS] [A2_Inc690] [A3_SS_reduced] and B [B1_SS] [B2_Inc690] [B3_SS_reduced],
- 2 upstream regions made of Zry for the Zn injection [Zry_Inj-Zn] and the ⁶⁰Co and Co injection [Zry_Inj-Co60],
- 1 upstream region for the alloy 690 pre-heater [Pre-heater],
- 2 downstream regions for the total purification of particles [Zry_Purif-part] and solubles [Zry_Purif-ion] to simulate the open loop (once-through system).

The variations in the simulated exposure conditions (see Figure 7) comply with the experimental exposure conditions (see Figure 5), except for the shutdown at the end of the test, which is not simulated. Thanks to the injection mechanism in medium Solubles (see Figure 3), the ⁶⁰Co injection at 200 Bq/kg in region [Zry_Inj-Co60] and the Zn injection at 10 ppb from 200 h in region [Zry_inj-Zn] can be simulated; the pH_{300°C} calculated by OSCAR/PHREEQCEA based on the boron and lithium concentrations varies between 6.9 and 7.6, and the temperature and dihydrogen are set at 285°C and 45 mL/kg respectively.

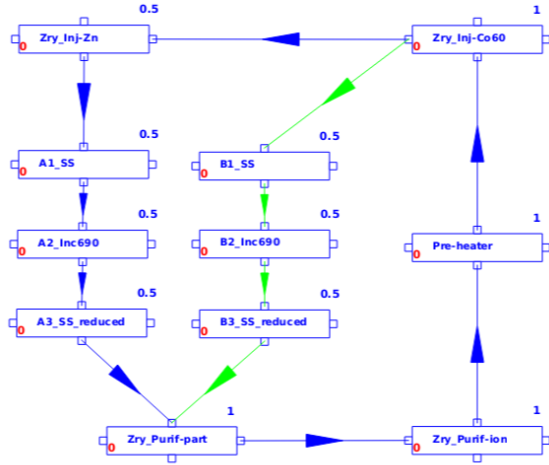


Figure 6. OSCAR v1.4 - Nodalization of the Studsvik testing loop.

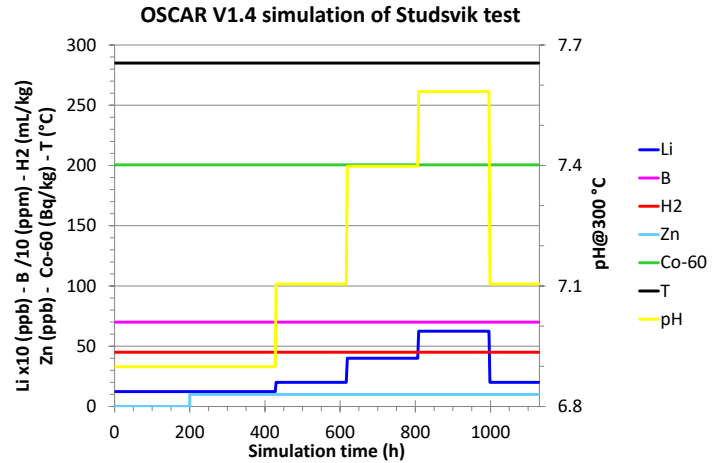


Figure 7. OSCAR v1.4 - Simulated exposure conditions of the Studsvik experiment.

The data entered into the OSCAR input file to define the test section is given in Table 3.

We consider that the flow is not established in tubes #1 (A1/B1) due to the test section inlet (relaxation length of 1 m) and in the inlet of tubes #3 (A3/B3) due to the reduced inner diameter (relaxation length of 1 cm). These considered relaxation lengths are close to the theoretical ones (Ribaud, 1957): 0.71 m ($0.06 \cdot Re \cdot D_H$ in laminar flow) and 1.1 cm ($0.8 \cdot Re^{1/4} \cdot D_H$ in turbulent flow) respectively.

The unknown Co content of SS 304L is set at 2000 ppm, which could correspond to the material of an ex-core pipe.

The initial thicknesses of the inner and outer oxides necessary for an OSCAR calculation are set to very low values (non-pre-oxidized and cleaned surfaces).

Table 3. OSCAR v1.4 - Tube data used for the OSCAR simulation of the Studsvik test.

Material	Tube #	Wet surface (cm ²)	Hydraulic diameter (mm)	Flow velocity (m.s ⁻¹)	Wall/Bulk temperat. (°C)	Relaxation length (m)	Initial composition of metal (weight %)					Initial thickness (nm)		Outer oxide open porosity (%)
							Cr	Mn	Fe	Co	Ni	Inner oxide	Outer oxide	
Alloy 690	2	265	16.87	0.005	285	0	29.7	0.27	9.7	0.007	60.323	0.1	5	95
SS 304L	1	160	17.0			1	18.72	1.65	68.93	0.2	10.5			
	3	13.2	1.4	0.74		0.01								

The calculated Reynolds number is 680 in laminar flow and 8300 in turbulent flow, which is consistent with the given values (see Table 2).

The diameter of soluble elements considered to calculate the mass transfer coefficient, h (see Eq. (21)), is 10 Å, which could correspond to an ion with its solvation shell.

The calibrated corrosion rate and the release rate (see section 2.4.1) for the two materials of the two 3-tube assemblies during the experiment are shown in Figure 8. The corrosion law used for this simulation is an empirical law depending on the material, time, pH, boron concentration, zinc concentration, saturation and temperature (Moorea law). The impacts of the pH and the Zn injection on the corrosion rates are low (about 15% for $pH_{300°C}$ between 6.9 and 7.6 and about 25% for Zn at the end of the simulation). The corrosion rates are around 2 mg.dm⁻².month⁻¹ for SS 304L and 0.1 mg.dm⁻².month⁻¹ for alloy 690 (NB: according to the Moorea law, the corrosion rate is an average value over the first two months and decreases over the next ten months).

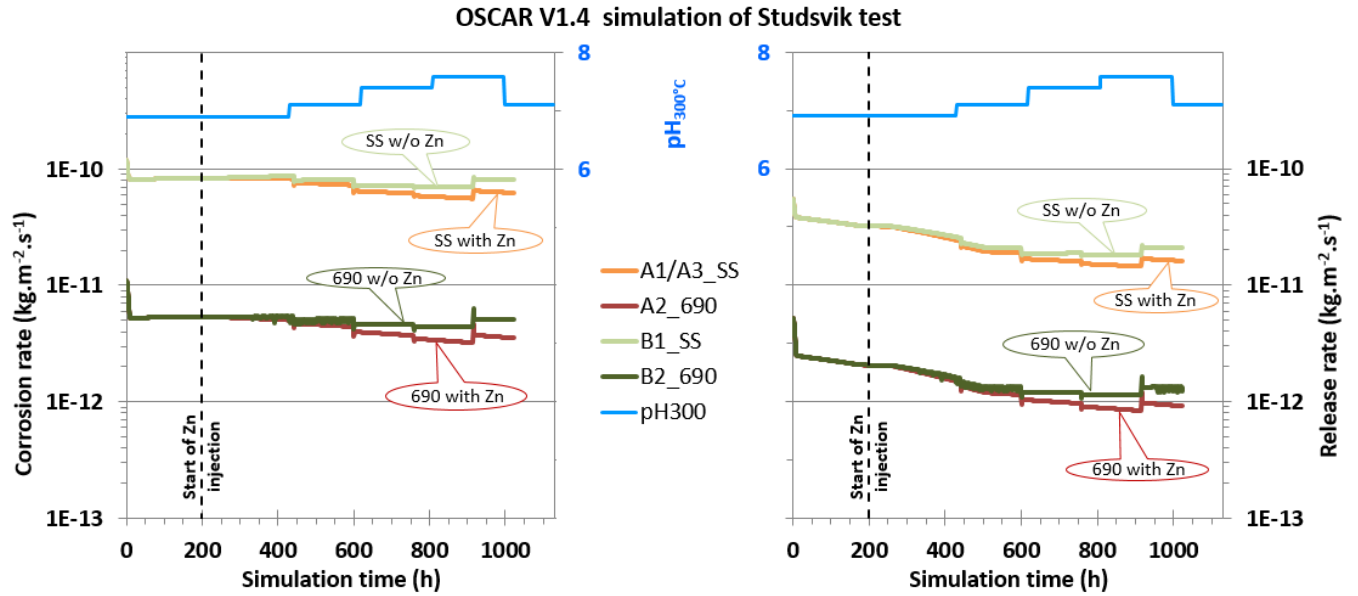


Figure 8. OSCAR v1.4 - Variations in the corrosion (left) and release (right) rates of the two materials for the two 3-tube assemblies during the Studsvik test simulation.

The variations in the calibrated dissolution surface reaction rates of cobalt chromite and cobalt ferrite during the Studsvik experiment (see section 2.5) are shown in Figure 9. The variations in our simulation are only due to the pH ($\mu_{\text{H}^+, \text{CoFe}_2\text{O}_4} = 1$, $\mu_{\text{H}^+, \text{CoCr}_2\text{O}_4} = 1$), the temperature and the H_2 concentration being constant. The dissolution surface reaction rate of cobalt chromite is 1000 times lower than that of cobalt ferrite. In the conditions of the experiment, the orders of magnitude are 10^{-15} - 10^{-14} $\text{mol}\cdot\text{m}^{-2}\cdot\text{s}^{-1}$ for cobalt chromite and 10^{-12} - 10^{-11} $\text{mol}\cdot\text{m}^{-2}\cdot\text{s}^{-1}$ for cobalt ferrite.

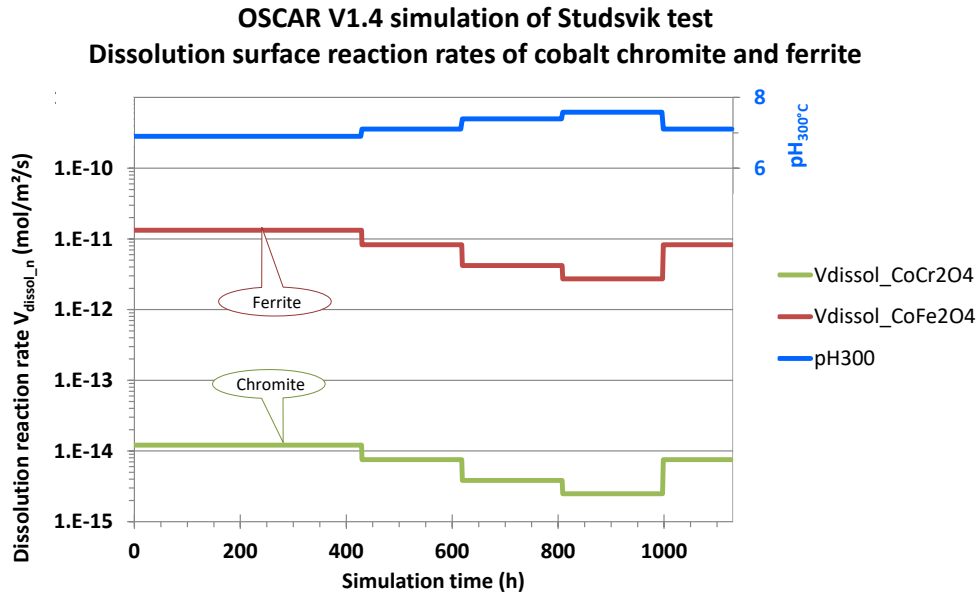


Figure 9. OSCAR v1.4 - Variation in the dissolution surface reaction rates of cobalt chromite ($V_{\text{dissol_CoCr}2\text{O}4}$) and cobalt ferrite ($V_{\text{dissol_CoFe}2\text{O}4}$) during the Studsvik test simulation.

3.3. Results

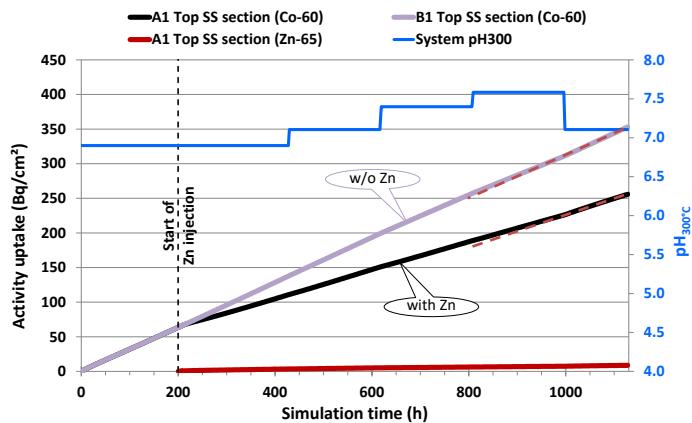
Figure 10 compares the ^{60}Co activity uptake on the sections of the two 3-tube assemblies calculated by OSCAR v1.4 against the one measured by Studsvik.

The time variation in the ^{60}Co uptake on the different tube sections measured are very well reproduced by the OSCAR calculation. In detail, the code reproduces the:

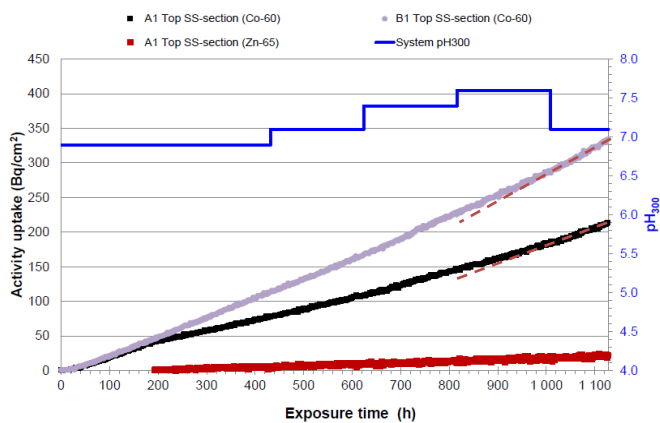
- Effect of the Zn concentration on ^{60}Co uptake on the SS 304L tube sections (see Figure 10 (1a) (1b)) and on the alloy 690 tube sections (see Figure 10 (2a) (2b)),
- Effect of the flow regime (laminar/turbulent) on ^{60}Co uptake on the SS 304L tube sections (see Figure 10 (3a) (3b)),
- Effect of the material on ^{60}Co uptake on the SS 304L and alloy 690 tube sections (see Figure 10 (3a) (3b)),
- Small changes in the ^{60}Co uptake's increasing slope, which is more or less pronounced due to pH variations: the very slight flattening of the increasing slope for the alloy 690 tube section due to the $\text{pH}_{300^\circ\text{C}}$ increase from 7.1 to 7.4-7.6 (see the green dotted lines on the graphs (2a) (2b) in Figure 10) and the slight steepening of the increasing slope for the SS tube sections due to the $\text{pH}_{300^\circ\text{C}}$ decrease from 7.6 to 7.1 at the end of the test (see the red dotted lines on the graphs (1a) (1b), (2a) (2b) and (3a) (3b) in Figure 10).

OSCAR v1.4 results

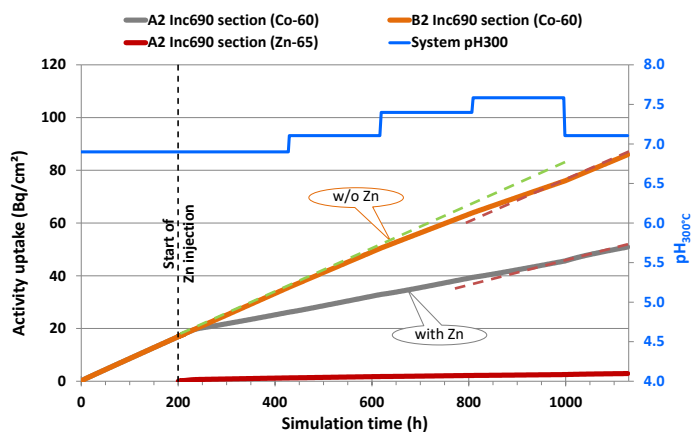
Studsвик measurements
(figures from (Öijerholm et al., 2016))



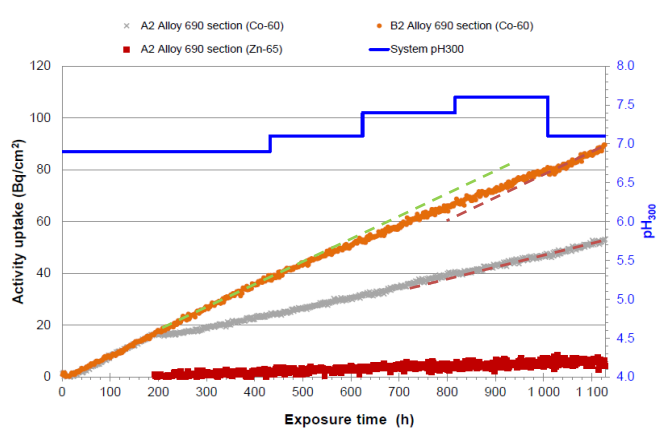
(1a)



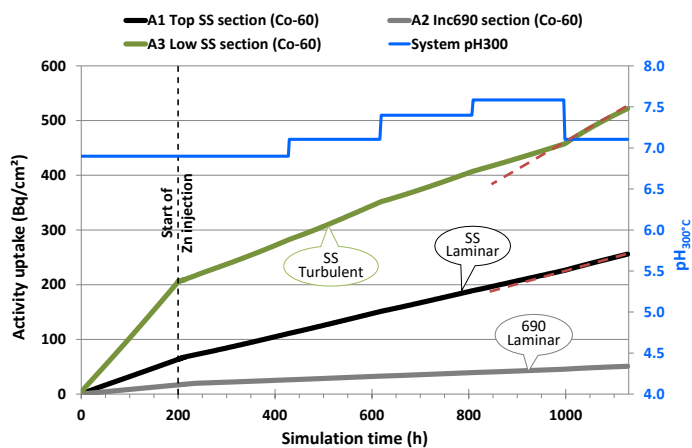
(1b)



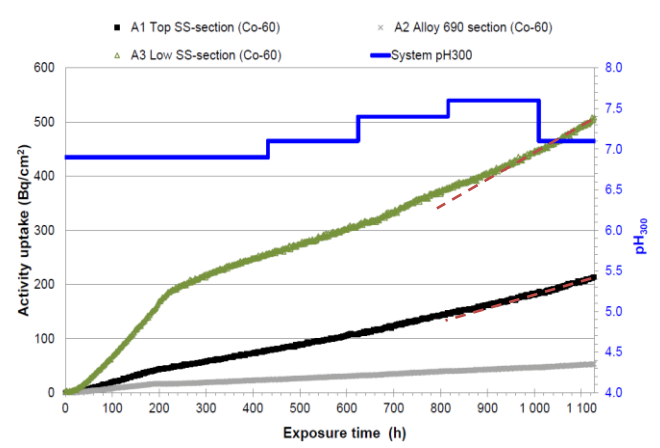
(2a)



(2b)



(3a)



(3b)

Figure 10. OSCAR v1.4 results (left) / Studsvik measurements from (Öijerholm et al., 2016) (right) - Activity uptake on the sections of the two 3-tube assemblies.

3.4. Discussion

3.4.1. Oxide speciation

The solid speciation of the inner and outer oxides is the key parameter for the dissolution-precipitation model. The solid speciation of the oxides on the SS (A1/B1) and alloy 690 (A2/B2) tube sections were calculated using OSCAR / PHREEQCEA (see section 2.4.4), which is shown in Figure 11 for a $\text{pH}_{300^\circ\text{C}}$ of 7.6 (simulation time = 960 h). This figure illustrates the effects of the material (SS/alloy 690) and Zn on the oxide composition.

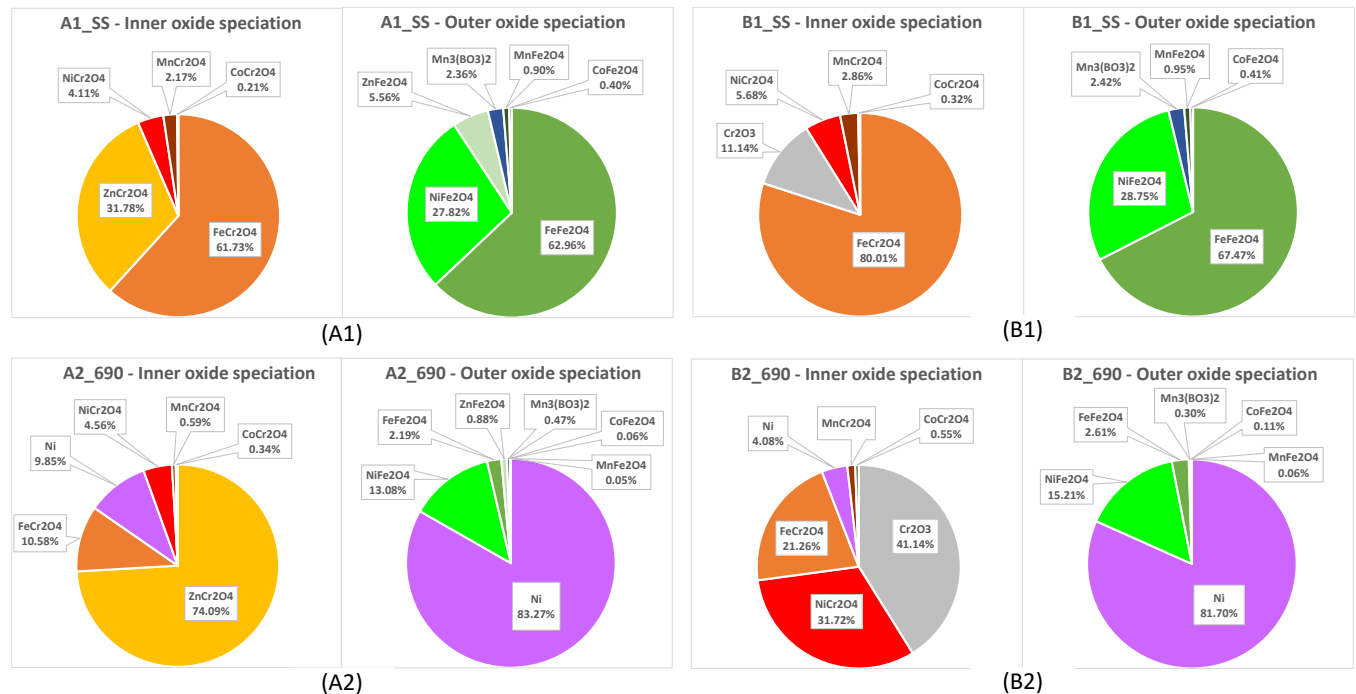


Figure 11. OSCAR v1.4 - Solid speciation (in mol-%) of the inner and outer oxides on the two-tube assembly sections (A1/A2 - B1/B2) at a simulation time of 960 h of the Studsvik test ($\text{pH}_{300^\circ\text{C}}$ of 7.6).

The calculated inner oxide is a Cr-rich layer (chromite / chromia) for both materials and the outer oxide is a Fe-rich layer (ferrite) for SS (A1 and B1) and a Ni-rich layer (Ni°) for alloy 690 (A2 and B2). For the sections exposed to Zn (A1 and A2), Zn is essentially present in the inner oxide layer, showing its strong affinity with chromite and not ferrite. These compositions are well known in PWR conditions (see, e.g., (Lister, 1993) or (Liu et al., 2011)). The oxide films formed on A1_SS were characterized for a similar experiment performed in the same test loop (Fager, 2015). However, some differences in the exposure conditions can be raised: $T = 325^\circ\text{C}$ vs 285°C ; $\text{pH}_{300^\circ\text{C}} = 7.4$ vs $6.9-7.6$; $[\text{Zn}] = 0-5-10$ ppb vs 10 ppb. The thin oxide film characterized by (Fager, 2015) corresponds to the Inner oxide medium in the OSCAR modelling and the precipitated oxides to the Outer oxide medium (see sections 2.2 and 2.4). The calculated thickness of the inner oxide on A1_SS is the same order of magnitude of the measured one: 29 nm (calculated) vs 15.9 ± 3.2 nm (measured). The comparison of the elemental compositions of the oxide layers are presented in Table 4. Considering the different exposure conditions (higher temperature, higher pH and lower Zn injection on average in (Fager, 2015)), the compositions are relatively close. The main differences concern the composition of the inner oxide, the calculated composition is lower in Fe and Ni and higher in Zn. For Co, which is the key element in this study, its content cannot be measured (trace element). On the other hand, despite the different conditions, the calculated and measured compositions of the outer oxide are comparable.

Table 4. OSCAR v1.4 results / Studsvik measurements (after (Fager, 2015)) - Elemental composition (in at-%) of the inner and outer oxides on A1_SS.

A1_SS composition (at-%)	O	Cr	Fe	Ni	Mn	Zn	Co	Si
	Inner oxide							
OSCAR calculation (simulation time = 960 h)	57.1	28.6	8.8	0.6	0.3	4.5	0.03	/
Measurements - min/max values (different exposure conditions) (Fager, 2015)	23.7 53.9	17.5 24.1	13.9 40.5	6.1 15.1	1.3 2.4	0.3 1.0	/	0.9 1.4
	Outer oxide							
OSCAR calculation (simulation time = 960 h)	57.4	0.0	36.6	3.9	1.1	0.8	0.06	/
Measurements - min/max values (different exposure conditions) (Fager, 2015)	35.0 55.2	0.0 9.6	25.2 47.1	3.5 10.8	0.0 1.3	0.0	/	0.0 1.7

Cobalt is in a single solid phase, i.e. cobalt chromite (CoCr_2O_4) in the inner oxide layer, and cobalt ferrite (CoFe_2O_4) in the outer oxide layer. The OSCAR simulation of this experiment thus enabled us to calibrate the dissolution surface reaction rates of the cobalt chromite and cobalt ferrite (see Figure 9). In fact, cobalt chromite is a constituent of a solid solution $(\text{Co}, \text{Fe}, \text{Ni}, \text{Mn}, \text{Zn})\text{Cr}_2\text{O}_4$ while cobalt ferrite is a constituent of a solid solution $(\text{Co}, \text{Fe}, \text{Ni}, \text{Mn}, \text{Zn})\text{Fe}_2\text{O}_4$. These solid solutions are mixed spinel oxides, e.g., for A1_SS according to the PHREEQCEA code:

- $\text{Co}_{0.0021}\text{Mn}_{0.0217}\text{Ni}_{0.0411}\text{Zn}_{0.3178}\text{Fe}_{0.6173}\text{Cr}_2\text{O}_4$ for the inner oxide layer,
- $\text{Co}_{0.0041}\text{Mn}_{0.0093}\text{Ni}_{0.2849}\text{Zn}_{0.0570}\text{Fe}_{0.6447}\text{Fe}_2\text{O}_4$ for the outer oxide layer.

To assess the impact of the Co content of SS304L, which is not known and set at 2000 ppm (see Table 3), a value of 1000 ppm was also used. Its impact on the ^{60}Co activity uptake on the SS304L sections is low, less than 4%.

3.4.2. Zn effect

According to the OSCAR code, the preferential incorporation of Zn in the inner oxide (chromite) is only due to the precipitation mechanism (see Eq. (21)). There is no specific model for Zn, i.e. the same precipitation / dissolution mechanism is applied to all metallic elements, including Zn, and the different behavioural patterns of the elements are only due to the different equilibrium concentrations in the coolant and the different dissolution velocities of the elements, which depend on the solid speciation, water chemistry and temperature. Like for Zn, the better affinity of Co for chromite than for ferrite is also reproduced by the OSCAR code, ^{60}Co uptake is preponderant on the inner oxide layer rather than on the outer oxide layer as shown in Figure 12, especially for alloy 690 (more than 99%). For SS without Zn, 60% of ^{60}Co is incorporated in the inner oxide layer for the laminar flow regime and 70% for the turbulent flow regime. Exposure to Zn has only an impact on the ^{60}Co uptake on the inner oxide layer and practically no impact on the ^{60}Co uptake on the outer oxide layer (see Figure 13 for section A1/B1).

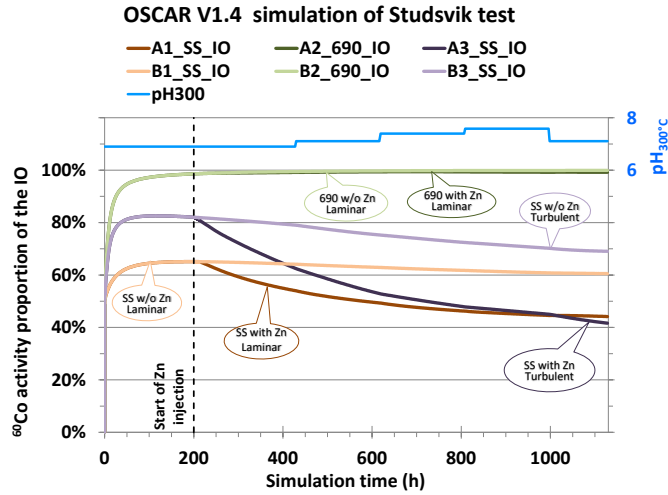


Figure 12. OSCAR v1.4 - Variation in the proportion of ^{60}Co activity in the inner oxide (IO) layer relative to the total ^{60}Co activity on the two 3-tube assemblies during the Studsvik test simulation.

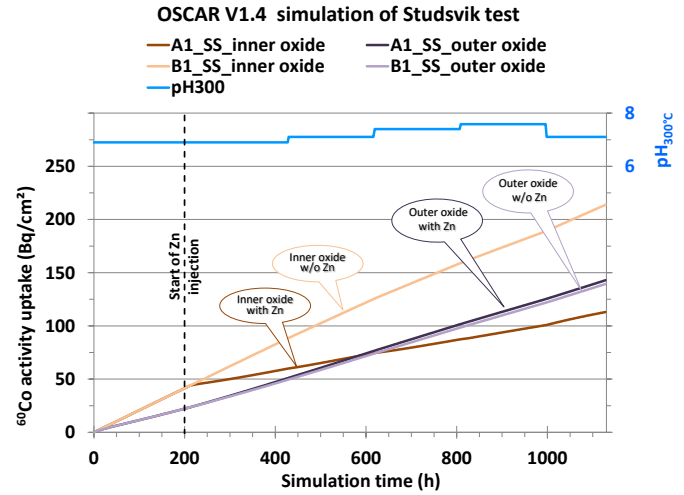


Figure 13. OSCAR v1.4 - Variation in the ^{60}Co activity uptake by the inner and outer oxide layers on the A1 and B1 tube sections during the Studsvik test simulation.

The lower ^{60}Co uptake on the inner oxide layer with Zn is due to the increase in one to two orders of magnitude in the equilibrium concentration of soluble Co with respect to this oxide (see Figure 14). This concentration remains inferior to the concentration of soluble Co, leading to a lower ^{60}Co precipitation rate⁹ (see Figure 15 for section A1/B1). However, the presence of Zn only has a slight or no impact on the Co equilibrium concentration in the coolant relative to the outer oxide layer of SS and alloy 690 (see Figure 14). According to the OSCAR v1.4 dissolution-precipitation model (see Eq. (21)), ^{60}Co precipitates on the outer oxide layer (see Figure 15) whereas the concentration of soluble Co is lower than the Co equilibrium concentration in solution relative to the outer oxide layer (unsaturated condition) during the first 100 hours of simulation (see Figure 14)¹⁰. The driving force of dissolution or precipitation for an isotope is $|f_{solid}^{i,elt} C_{eq}^{elt} - f_{fluid}^{i,elt} C^{elt}|$ (see section 2.4.4) rather than $|C_{eq}^{elt} - C^{elt}|$, which is the driving force for an element.

⁹ Depending on the conditions, the equilibrium concentration of soluble Co in the coolant with respect to the inner oxide layer can exceed the concentration of soluble Co during Zn exposure, leading to the dissolution of Co and thus a decrease in the ^{60}Co activity of the inner oxide layer (Bultot et al., 2016).

¹⁰ Note that the soluble calculated Co concentration (black curve in Figure 14) is about 9 ppt as dosed (see Table 1).

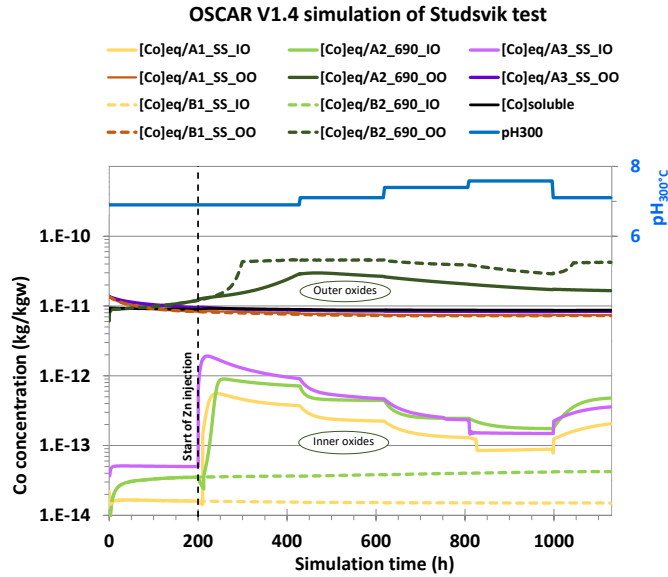


Figure 14. OSCAR v1.4 - Variations in the soluble Co concentration and the Co equilibrium concentrations in the coolant with respect to the considered oxide (inner oxide (IO) or outer oxide (OO)) in the two 3-tube assemblies during the Studsvik test simulation.

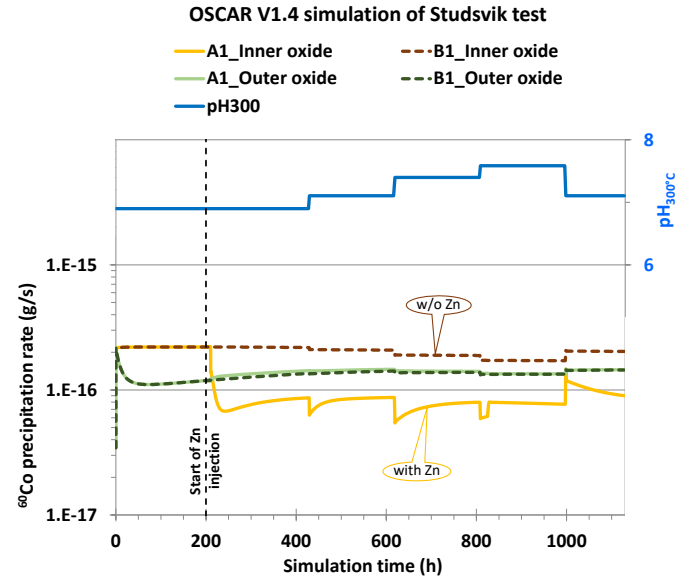


Figure 15. OSCAR v1.4 - Variations in the ^{60}Co precipitation rate on the inner and outer oxide layers of the A1 (with Zn) and B1 (without Zn) tube sections during the Studsvik test simulation.

To assess the impact of the decrease in corrosion rate due to the presence of Zn (see Figure 8), an OSCAR calculation without the corrective factor of Zn in the Moorea law was also performed. The impact on the ^{60}Co activity uptake is low for both materials, less than 7%, showing that the main impact of Zn is via the precipitation-dissolution rate and not via the corrosion rate.

The uniform ^{60}Co surface activity in a PWR primary system is also due to the deposition of particles on the outer oxide layer on which Zn has no impact, which explains why the impact of Zn injection on ^{60}Co contamination is unclear (Tigeras et al., 2008) and depends on the ^{60}Co activity distribution in the inner oxide and deposit / outer oxide layers, i.e. the impact can be positive, neutral or negative (Bultot et al., 2016). In the same way, it would be hasty to conclude that a $\text{pH}_{300^\circ\text{C}}$ of 7.6 is the optimum level for the PWR primary coolant's chemistry because the pH effect on ^{60}Co uptake is only slight (see section 3.3) and ^{60}Co uptake is just one aspect of the complex contamination transfer process (see section 2.1). The OSCAR code is thus a powerful tool for determining the optimum water chemistry because it can take into account different aspects of the contamination transfer process in nuclear reactor systems.

3.4.3. Limiting kinetic parameter

Figure 16 and Figure 17 show the variations in the mass transfer coefficient of soluble Co, $h = 1/R_{\text{wall-bulk}}^{\text{fluid}}$ ¹¹ and in the dissolution velocity for Co, $v_{\text{dissol}}^{\text{Co}} = 1/R_{\text{solid-fluid}}^{\text{elt}}$, with respect to the inner and outer oxide layers of the two 3-tube assemblies. They were used to determine the limiting kinetic parameter of the dissolution-precipitation mechanism between the transfer resistance in the fluid between the wall and the bulk, $R_{\text{wall-bulk}}^{\text{fluid}}$, and the transfer resistance at the interface solid-fluid, $R_{\text{solid-fluid}}^{\text{elt}}$, (see Eq. (21)).

¹¹ The diffusion of Co through the outer oxide layer, which consists of small scattered crystallites on the Studsvik tube sections, is not limiting for precipitation on the inner oxide layer. These small scattered crystallites are simulated in the OSCAR code by an outer oxide layer with high open porosity (see Table 3).

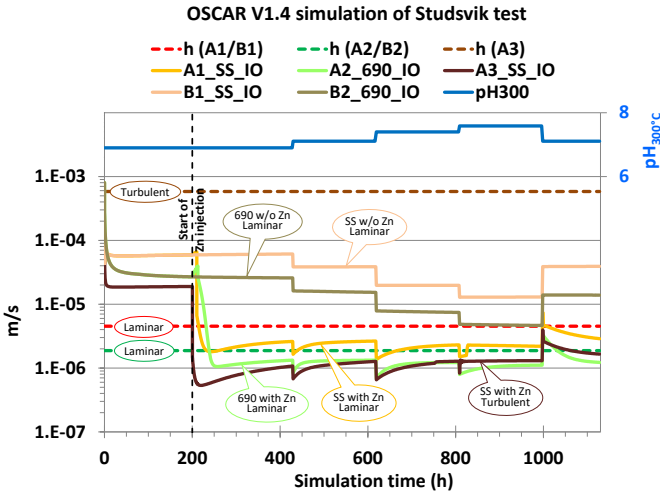


Figure 16. OSCAR v1.4 - Variations in the dissolution velocity of Co for the inner oxide (IO) and mass transfer coefficient of soluble Co (h) in the two 3-tube assemblies during the Studsvik test simulation.

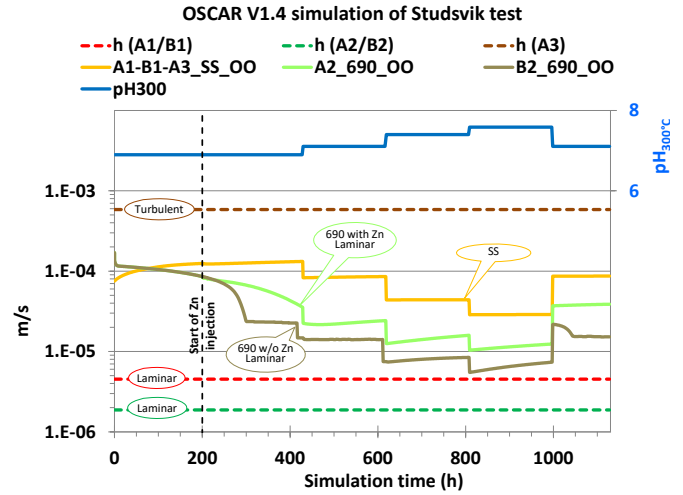


Figure 17. OSCAR v1.4 - Variations in the dissolution velocity of Co for the outer oxide (OO) and mass transfer coefficient of soluble Co (h) in the two 3-tube assemblies during the Studsvik test simulation.

For the laminar flow regime of this experiment (tube sections A1/B1 and A2/B2), the mass transfer coefficient h controls the kinetics of Co precipitation on the outer oxide layers and on the inner oxide layer except in the presence of Zn. In these exceptional cases, the mass transfer coefficient and the dissolution velocity have the same order of magnitude. Note that the difference in the mass transfer coefficient in the tube sections between A1/B1 and A2/B2 is due to the difference in the relaxation length (see Table 3).

For the turbulent flow regime of this experiment, however, the limiting kinetic parameter of the dissolution-precipitation mechanism is the dissolution velocity of Co regardless of the pH and Zn exposure. Therefore, we recommend performing experiments in a turbulent flow regime to determine the surface reaction rate of dissolution or precipitation in PWR primary coolant conditions. In this way, it can be made sure that the limiting kinetic parameter is not the mass transfer coefficient in the fluid.

Note that Zn has an impact on the dissolution velocity of Co for the inner oxide layer and a slight or no impact for the outer oxide layer. This is due to the effect of Zn on the equilibrium concentrations of soluble Co in the coolant with respect to the inner or outer oxide layers (see Figure 14 and Figure 15).

4. Conclusion

The CEA has spent almost 50 years developing the PACTOLE code, now known as the OSCAR code, used to predict the transfer of ACPs in nuclear systems. Improvements were made to the dissolution-precipitation model in the latest version of this code, OSCAR v1.4, i.e.:

- The expressions of the surface dissolution and precipitation mechanisms are now the same (the precipitation rate is a function of the dissolution velocity);
- The dissolution velocity of an element [$\text{m}\cdot\text{s}^{-1}$] is a function of the dissolution surface reaction rates of solid phases containing this element [$\text{mol}\cdot\text{m}^{-2}\cdot\text{s}^{-1}$], which depends on the temperature, pH and partial pressure of dihydrogen or dioxygen;
- The new precipitation / dissolution model describes the incorporation of isotopes in the oxide layers, even in unsaturated conditions for the element. This is essential for simulating the behaviour of cobalt isotopes.

These improvements and the OSCAR chemistry module, PHREEQCEA, which determines the solid speciation and the equilibrium concentrations of each element in aqueous solutions, enable the OSCAR v1.4 code to calculate the uptake of minor species, such as a Co isotope, into the solid solutions of the inner and outer oxide layers. Thus, the OSCAR v1.4 code accurately simulates the measured impact of the pH, Zn injection and flow regime on ^{60}Co uptake on stainless steel and alloy 690 as highlighted in an experiment performed by Studsvik

Nuclear AB. The main adjusted parameters are the dissolution surface kinetic constant k_n and the proton reaction order $\mu_{H^+,n}$ for cobalt ferrite and chromite.

This new version of the OSCAR code provides users with a powerful tool for analysing the behaviour of ACPs in different conditions and thus for predicting and explaining this behaviour (see, e.g., (Jobert et al., 2019)). Since it takes into account different aspects of the contamination transfer process, the OSCAR code can be used to determine the optimum water chemistry of nuclear reactor systems. The next improvement of the OSCAR code is the development of a deposition model for colloids with respect to activity build-up on surfaces due to ACPs (Cherpin et al., 2022a; Cherpin et al., 2022b).

Acknowledgements

The authors would like to thank Johan Öijerholm from Studsvik Nuclear AB for providing additional information on the Studsvik experiment.

Funding

This work was financed by the CEA, EDF and Framatome (France).

References

- Beal, S.K., 1970. Deposition of particles in turbulent flow on channel or pipe walls. *Nuclear science and engineering* 40, 1-11.
- Beslu, P., Leuthrot, C., 1990. PACTOLE-PROFIP: two codes allowing prediction of the contamination of PWR primary circuits, *Revue Générale Nucléaire*, pp. 552-554.
- Bretelle, J.L., Rocher, A., Berger, M., Dacquait, F., Rosset, R., 2002. Study of various chemical species behaviour for contamination risk, *Int. Conf. on Water Chemistry in Nuclear Reactors Systems, NPC 2002*. SFEN, Avignon (France).
- Bultot, M., Dacquait, F., Tevissen, E., Schildermans, K., Lecocq, R., 2016. Zinc effect on the primary circuit contamination of a Belgian PWR using the OSCAR V1.3 code, *Int. Conf. on Water chemistry in nuclear reactors systems, NPC 2016*. NI, Brighton (UK).
- Cherpin, C., Lister, D.H., Dacquait, F., Liu, L., Weerakul, S., 2022a. Magnetite (Fe₃O₄) and nickel ferrite (NiFe₂O₄) zeta potential measurements at high temperature: Part I—Design, materials and preliminary characterization of an apparatus implementing the streaming potential method. *Colloids and Surfaces A: Physicochemical and Engineering Aspects* 646, 128961.
- Cherpin, C., Lister, D.H., Dacquait, F., Weerakul, S., Liu, L., 2022b. Magnetite (Fe₃O₄) and nickel ferrite (NiFe₂O₄) zeta potential measurements at high temperature: Part II – Results, study of the influence of temperature, boron concentration and lithium concentration on the zeta potential. *Colloids and Surfaces A: Physicochemical and Engineering Aspects* 647, 129030.
- Cleaver, J.W., Yates, B., 1972. Mechanism of Detachment of Colloidal Particles from a Flat Substrate in a turbulent Flow. *Journal of Colloid and Interface Science* 44.
- Dacquait, F., Andrieu, C., Guinard, L., Bretelle, J.L., Bardet, F., Rocher, A., Brun, C., 2004. Status of primary system contamination in French PWRs, *Int. Conf. on Water chemistry in nuclear reactors systems, NPC 2004*, San Francisco (USA).
- Dacquait, F., Bultot, M., Pipet, G., Francescato, J., Broutin, F., Benfarah, M., Mondit, P., 2016. 110mAg behaviour in PWRs: Lessons learnt from the EMECC campaigns, *Int. Conf. on Water chemistry in nuclear reactors systems, NPC 2016*. NI, Brighton (UK).
- Dacquait, F., Francescato, J., Galassi, G., Broutin, F., Gherrab, M., You, D., Jobert, T., Engler, N., 2018. The OSCAR V1.4 code: A new dissolution-precipitation model to better simulate the corrosion product transfer in nuclear cooling systems, *Int. Conf. on Water chemistry in nuclear reactors systems, NPC 2018*, San Francisco (USA).
- Dacquait, F., Genin, J.B., Brissonneau, L., 2020. Modelling of the contamination transfer in nuclear reactors: The OSCAR code - Applications to SFR and ITER, *Challenges for Coolants in Fast Neutron Spectrum Systems*. IAEA, Vienna (Austria), pp. 77-83.

Dacquait, F., Genin, J.B., Francescato, J., Benier, G., Galassi, G., Broutin, F., Gherrab, M., Tevissen, E., You, D., Jobert, T., Chirent, T., Engler, N., Mariet, C., 2021. The OSCAR code: a simulation tool to assess the PWR contamination for decommissioning, Int. Conf. on Decommissioning Challenges: Industrial Reality, Lessons learned and Prospects, DEM 2021. SFEN, Avignon (France).

Eimecke, R., Anthoni, S., 1988. Ensemble de Mesure et d'Etude de la Contamination des Circuits (EMECC), 7th Int. Conf. on Radiation Shielding. UKAEA, Bournemouth (UK).

Fager, C., 2015. Structural Characterization of Oxide Films Formed on Stainless Steel of Type 304L in Simulated PWR Primary Water. Chalmers University of Technology (Sweden).

Ferrer, A., 2013. Modélisation des mécanismes de formation sous ébullition locale des dépôts sur les gaines de combustible des Réacteurs à Eau sous Pression conduisant à des activités volumiques importantes. Université de Strasbourg (France).

Genin, J.B., Marteau, H., Daquait, F., Bénier, G., Francescato, J., Broutin, F., Nguyen, F., Girard, M., Noirot, L., Maillard, S., Marelle, V., Bouloré, A., You, D., Plancque, G., Ranchoux, G., Bonnefon, J., Bonelli, V., Bachet, M., Riot, G., Grangeon, F., 2010. The OSCAR code package: a unique tool for simulating PWR contamination, Int. Conf. on Water Chemistry of Nuclear Reactors Systems, NPC 2010. CNS, Quebec (Canada).

Girard, M., Daquait, F., Genin, J.-B., Ranchoux, G., Riot, G., 2012. Experimental study of particle deposition kinetics in the primary circuit of the CIRENE loop and comparison with OSCAR V1.2 code simulations, Int. Conf. on Water chemistry in nuclear reactors systems, NPC 2012. SFEN, Paris (France).

IAEA, 2012. Modelling of transport of radioactive substances in the primary circuit of water cooled reactors, IAEA-TECDOC-1672, International Atomic Energy Agency, Vienna (Austria).

Jobert, T., Cherpain, C., Daquait, F., Genin, J.B., Tevissen, E., 2019. Study of the impact of three B/Li coordinated chemistries on the cobalt 58 surface contamination of a French PWR using the OSCAR code v1.4, 27th Int. Conf. on Nuclear Engineering, ICONE-27, Ibaraki (Japan).

Lister, D.H., 1993. Activity transport and corrosion processes in PWRs. Nuclear Energy 32, 103-114.

Liu, X., Wu, X., Han, E.-H., 2011. Influence of Zn injection on characteristics of oxide film on 304 stainless steel in borated and lithiated high temperature water. Corrosion Science 53, 3337-3345.

Marchetti-Sillans, L., 2007. Corrosion généralisée des alliages à base nickel en milieu aqueux à haute température : apport à la compréhension des mécanismes, Génie des Procédés. Ecole Nationale Supérieure des Mines de Saint-Etienne (France), p. 272.

Marchetto, C., 2002. Modélisation et simulation numérique du transport des produits de corrosion dans le circuit primaire des réacteurs à eau pressurisée, Mécanique Energétique. Université de Provence Aix-Marseille I (France), p. 212.

Michell, S.J., 1970. Fluid and particle mechanics, Pergamon press Ltd.

Öijerholm, J., Bengtsson, B., Gillén, P., Svanberg, P., 2016. Influence of pH, Temperature and Flow Velocity on Co-60 Uptake on Alloy 690 and Stainless Steel in Simulated PWR Chemistry, Int. Conf. on Water chemistry in nuclear reactors systems, NPC 2016. NI, Brighton (UK).

Öijerholm, J., Bengtsson, B., Gillén, P., Svanberg, P., Chen, J., 2014. Uptake of Co-60 on Alloy 690 and Stainless Steel Type 304L Surfaces in Simulated PWR Primary Chemistry, Int. Conf. on Water Chemistry in Nuclear Reactors Systems, NPC 2014, Sapporo (Japan).

Parkhurst, D.L., Appelo, C.A.J., 2013. Description of Input and Examples for PHREEQC Version 3 - A Computer Program for Speciation, Batch-Reaction, One-Dimensional Transport, and Inverse Geochemical Calculations, in: Survey, U.G. (Ed.), Denver (USA).

Plancque, G., You, D., Blanchard, E., Mertens, V., Lamouroux, C., 2011. Role of chemistry in the phenomena occurring in nuclear power plants circuits, Int. Conf. on Advances in nuclear Power Plants, ICAPP 2011, Nice (France).

Plancque, G., You, D., Mertens, V., Blanchard, E., 2008. Experimental study and modeling of the corrosion product dissolution. Applications to PWR conditions (nominal operating and cold shutdowns conditions), Int. Conf. on Water Chemistry of Nuclear Reactors Systems, NPC 2008. VGB, Berlin (Germany).

Ponting, A.C., Rodliffe, R.S., 1983. Intrinsic filtration and retarded deposition for the control of colloidal corrosion product deposition on PWR fuel, in: BNES (Ed.), Int. Conf. on Water Chemistry of Nuclear Reactor System, Bournemouth (UK), pp. 43-51.

Poulson, B., 1983. Electrochemical measurements in flowing solutions. *Corrosion Science* 23, 391-430.

Ribaud, G., 1957. Convection laminaire et convection turbulente. *La Houille Blanche*, 12-18.

Rodliffe, R.S., Polley, M.V., Thornton, E.W., 1987. Modelling the behaviour of corrosion products in the primary heat transfer circuits of pressurized water reactors. A review of principles. IAEA, Vienna (Austria), pp. 105-164.

Tigeras, A., Dacquait, F., Viricel, L., Segura, J.C., Guinard, L., Bretelle, J.L., Rocher, A., 2008. Complete Analyse of Zinc injection impact at BUGEY 2&4, Int. Conf. on Water chemistry in nuclear reactors systems, NPC 2008. VGB, Berlin (Germany).